

SRG/eROSITA discovery of 164 s pulsations from the SMC Be/X-ray binary XMMU J010429.4–723136

S. Carpano¹, F. Haberl¹, C. Maitra¹, M. Freyberg¹, K. Dennerl¹, A. Schworer², A. H. Buckley³, and I. M. Monageng^{3,4}

¹ Max-Planck-Institut für extraterrestrische Physik, Gießenbachstraße 1, 85748 Garching, Germany
e-mail: scarpano@mpe.mpg.de

² Leibniz Institut für Astrophysik Potsdam, An der Sternwarte 16, D-14482 Potsdam, Germany

³ South African Astronomical Observatory, P.O. Box 9, Observatory, Cape Town 7935, South Africa

⁴ Department of Astronomy, University of Cape Town, Private Bag X3, 7701 Rondebosch, South Africa

Received April XX, 2021; accepted XX XX, 2021

ABSTRACT

Context. The Small Magellanic Cloud (SMC) is hosting many known high-mass X-ray binaries, all but one (SMC X-1) having Be companion stars. Through the calibration and verification phase of eROSITA on board the SRG spacecraft, the Be/X-ray binary XMMU J010429.4–723136 was in the field of view during observations of the supernova remnant 1E0102.2-7219, used as calibration standard.

Aims. We report here a time and spectral analysis of XMMU J010429.4–723136, based on two eROSITA observations of the field, performed on 2019 November 7–9. We also reanalyse the OGLE light curve for that source, in order to determine the orbital period.

Methods. The search for pulsations (from the X-ray data) and for the orbital period (from the OGLE data) is done via Lomb-Scargle periodogram analysis. X-ray spectral parameters and fluxes are retrieved from the best-fit model.

Results. We detected for the first time, the pulsations of XMMU J010429.4–723136 at a period of \sim 164 s, and therefore designate the source as SXP 164. From the spectral fitting, we derive a source flux of $\sim 1 \times 10^{-12}$ erg s $^{-1}$ cm $^{-2}$ for both observations, corresponding to a luminosity of $\sim 4 \times 10^{35}$ erg s $^{-1}$ at the distance of the SMC. Furthermore, reanalysing the OGLE light curve including the latest observations, we found a significant periodic signal at 22.3 d likely being the orbital period, which is shorter than the previously-reported values.

Key words. galaxies: individual: Small Magellanic Could – stars: neutron – X-rays: binaries – X-rays: individual: SXP 164–stars: emission-line, Be

1. Introduction

High-mass X-ray binaries (HMXBs) are close systems composed of an early type star and a compact object being either a neutron star or a black hole (occasionally a white dwarf). Be or B[e]-type stars, are a subset of B-type stars where one or more Balmer emission lines are found in the optical spectrum, and are believed to possess an equatorialcretion disc, possibly causing regular X-ray outbursts at periastron passage of the compact object due to enhanced mass accretion (see e.g. Reig 2011, for a review). A large number of such systems was found in the Small Magellanic Cloud (SMC). The latest comprehensive catalogue was published by Haberl & Sturm (2016) and collects 121 high-confidence HMXBs (the vast majority with Be companion stars). For about half of the sample X-ray pulsations were discovered with periods ranging from a fraction to a few thousands of seconds. Pulse periods of the 62 Be/X-ray binaries have a bi-modal distribution peaking around 10 s and 250 s (Haberl & Sturm 2016). For the other sources, pulse periods are still not reported, one of them being XMMU J010429.4–723136, identified as source number 132 in their Table A.1. The source was already mentioned as source number 3285 in the previous *XMM-Newton* catalogue of X-ray point sources in the SMC (Sturm et al. 2013, in their Table 5).

XMMU J010429.4–723136 was confirmed as a Be star (more precisely of type B1 V) by McBride et al. (2017) using spectra recorded with the Anglo-Australian Telescope on 2012

July 7–8, in the wavelength range [4025–4775] Å. Large X-ray variability was already reported by Maggi et al. (2013) comparing a series of *Swift*/XRT observations, where the luminosity ranged from 2.8 to 12.4×10^{35} erg s $^{-1}$ on MJD 56627.09 to 56643.31 (December 2013), with a previous *XMM-Newton* observation on MJD 55149.1 (November 2009), where only an upper limit a factor of \sim 400 lower could be extracted. The source is not reported in the RXTE Catalogue of SMC pulsars from Galache et al. (2008), based on 9 yr of SMC survey (starting in 1997), but was detected by Chandra in August 2002 with a luminosity of 1.4×10^{35} erg s $^{-1}$ (Rajoelimanana et al. 2011a).

The Optical Gravitational Lensing Experiment (OGLE) light curve of XMMU J010429.4–723136, in the *I*-band, is shown in McBride et al. (2017), as source XMM 3285, covering the epoch from MJD 55346 to MJD \sim 57400 (May 2010 to January 2016). The source was in a low state for \sim 600 d and then increased towards a stable higher state ($\Delta I=1.25$ mag). A period of 29.75 d was found in the data covering the short time interval MJD 55650–56100 (and after some detrending). This is somewhat lower than the strong modulation of 37.15 ± 0.02 d claimed by Rajoelimanana et al. (2011a) and associated later by Schmidtke et al. (2013), with aliasing of a possible shorter period modulation of 0.972 d. This last short period was interpreted as being non-radial pulsations from the Be star. Note that in both works from Rajoelimanana et al. (2011a) and Schmidtke et al. (2013), the source is erroneously named as SXP 707 from a period dis-

covered in the Chandra data at 707 s. That period is actually the satellite dithering period, with the source, located at the rim of a CCD, moving in and out of the detector (as already clarified in Haberl & Sturm 2016).

In this paper, we report the discovery of X-ray pulsations for XMMU J010429.4–723136 with a period of 164 s and rename the source as SXP 164 following the terminology first proposed by Coe et al. (2005) (where SXP stands for Small Magellanic Cloud X-ray Pulsar, followed by the pulse period in seconds to three significant figures). The discovery was already briefly announced by Haberl et al. (2019). We also report the detection of a strong signal at 22.3 d in the OGLE light curve, that we interpret as the possible orbital period.

2. Observations and data reduction

The X-ray observations were performed during the calibration and verification phase of eROSITA (Predehl et al. 2021), from UTC 2019-11-07 16:59:49 to 2019-11-08 13:00:10 (obsID 700001) and 2019-11-09 00:59:40 to 2019-11-09 21:00:10 (obsID 700003), each observation for a total exposure of ~ 72 ks. During the first observation, the source was far off-axis (at an angle of $29.7'$) and covered by only five cameras (telescope modules TM1,3,4,5,6), while the source was located in the field-of-view of all seven cameras in the second observation (with an off-axis angle of $26.7'$). The data were reduced using the eROSITA Standard Analysis Software System pipeline (eSASS, Brunner et al. , submitted), version eSASSusers_201009. The software determines good time intervals, corrupted events and frames, dead times, masks bad pixels, projects the photons onto the sky, and applies pattern recognition and energy calibration. Source and background extraction regions were defined as a circle (radius $70''$) and an annulus (radii $90''$ and $150''$), respectively. The regions were centered on the *XMM-Newton* coordinates of the source (RA, DEC)= (01:04:29.42, -72:31:36.5), derived in Sturm et al. (2013).

Optical spectroscopy of XMMU J010429.4–723136 was undertaken on 2019-11-24 using the Robert Stobie Spectrograph (RSS, Burgh et al. 2003) on the Southern African Large Telescope (SALT, Buckley et al. 2006) under the transient follow-up program. The PG2300 VPH grating was used, which covered the spectral region 6100 – 6900 Å at a resolution of 1.2 Å. A single 1200 s exposure was obtained, starting at 19:40:08 UTC.

The X-Ray variables OGLE Monitoring (XROM) system provides real-time photometry (*I*-band) of optical counterparts of X-ray sources¹ located in the fields observed in the OGLE-IV survey (Udalski 2008), with roughly daily sampling. To date, data available for SXP 164 cover the period from MJD 55346 (2010-05-30) to MJD 58870 (2020-01-21).

3. Data analysis and results

3.1. eROSITA

3.1.1. X-ray light curves and pulse period search

The background-subtracted and vignetting-corrected light curves of SXP 164 from the two observations (obsIDs 700001 and 700003) performed during the calibration phase are shown in Fig. 1. They were produced using the eSASS task `srctool` in the energy band 0.2–5.0 keV and with a bin size of 2000 s. The mean count rate, shown by the red lines, is 0.11 ct/s for

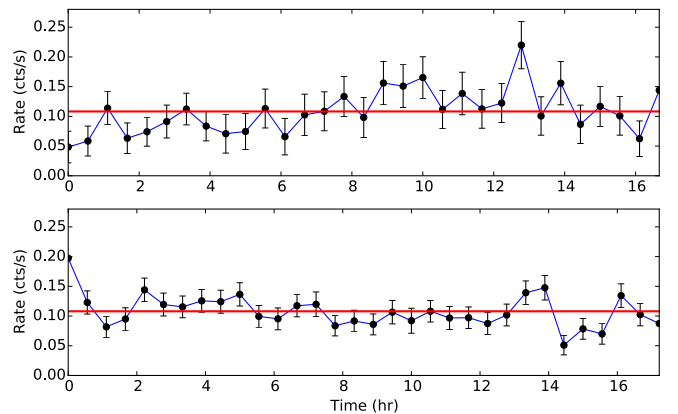


Fig. 1. eROSITA light curve of SXP 164, during obsID 700001 (top) and 700003 (bottom), rebinned at 2000 s, extracted in the 0.2–5.0 keV band. The red lines indicate the mean value, of 0.11 cts/s, in both observations.

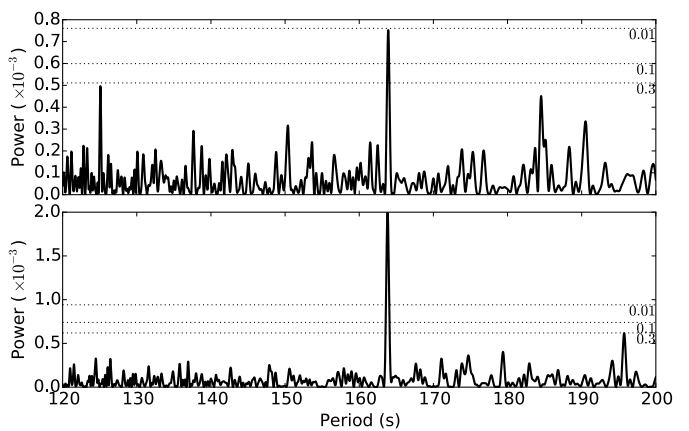


Fig. 2. Lomb-Scargle periodogram for the two eROSITA observations (obsID 700001 and 700003), using light curves binned at 2 s. The best periods are 163.91 s and 163.83 s respectively, with the $1-\sigma$ uncertainty derived from the Gaussian fit of 0.17 s and 0.18 s.

both observations. The portion of the light curves where all available cameras are operating simultaneously have almost the same length in both observations (~ 17 h, more exactly 60 ks and 62 ks). No large variability is observed during the single observations.

The pulse period search is performed using a Lomb-Scargle analysis (Lomb 1976; Scargle 1982), in the energy band 0.2–5 keV (where the signal is stronger) and in the period range 120–200 s (a larger period interval was initially used during the first screening). Figure 2 shows the periodogram corresponding to the two observations, performed on background-subtracted light curves binned at 2 s. Strong peaks are found with maxima at 163.91 s and 163.83 s, respectively and with a $1-\sigma$ uncertainty of 0.17 s and 0.18 s, derived from a Gaussian fit to the highest peak. The two pulse period values are therefore consistent taking into account the uncertainties. The confidence levels (given at 68%, 90% and 99%) are derived using the block-bootstrap method as explained in Carpano et al. (2017). It consists first in simulating 1000 light curves, each by splitting the original light curves in blocks of ~ 650 s and randomly shuffling the blocks, and then retrieving the corresponding periodogram maxima.

Figure 3 shows the light curves of SXP 164 folded at their best period, with the best fit sine function overlaid. The pulse profile, better defined in the second observation where more pho-

¹ <http://ogle.astroww.edu.pl/ogle4/xrom/xrom.html>

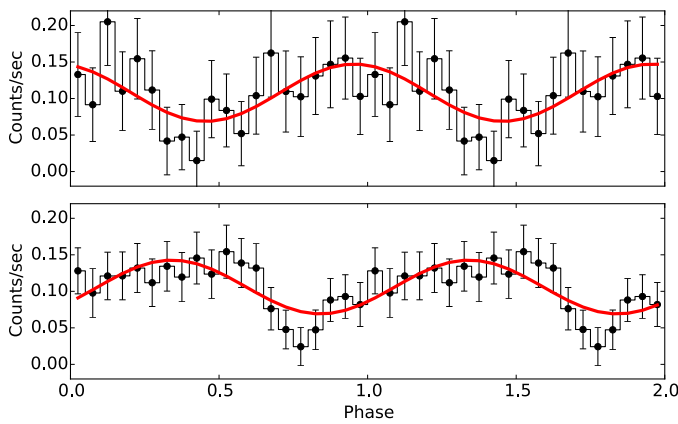


Fig. 3. Folded eROSITA light curve of SXP 164, during obsID 700001 (top) and 700003 (bottom), extracted in the 0.2–5.0 keV band, with best-fit sine function overlaid. Phase 0 corresponds to the start of each observation.

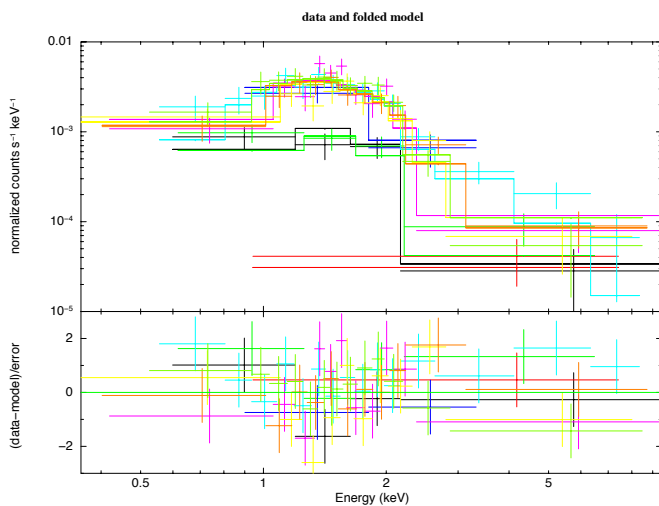


Fig. 4. Simultaneous spectral fit of SXP 164, for obsID 700001 (4 cameras) and 700003 (5 cameras), using an absorbed power-law model ($\text{TBabs}^*\text{TBvarabs}^*\text{power}$), and the corresponding residuals.

tons are available, looks non sinusoidal and slightly asymmetric. The pulsed fraction, defined as $PF = \frac{\max - \min}{\max + \min} \times 100$ (%), with \max and \min being the maximum and minimum of the folded light curves, are 86.3% and 72.9% for the first and second observation, respectively. Phase 0 corresponds to the start of each observation and are both separated by 120767 s, while their first minima by 120824 s. Assuming an integer number of cycles between the two minima, which could be 736, 737 or 738 cycles, the corresponding pulse period (assuming it is constant over this timescale) would be 164.16 s, 163.94 s or 163.72 s, respectively. Alternatively, the period search can also be performed on both data sets jointly, leading to a best period of 163.89 ± 0.19 s.

3.1.2. Spectral analysis

The eROSITA spectra of SXP 164 were fitted with PyXspec² in the full 0.2–10 keV energy band, for the two observations simultaneously (fitting the data for the two observations separately would lead to similar spectral parameters but with larger uncer-

Table 1. Spectral parameters resulting from the simultaneous fit to the eROSITA spectra during obsID 700001 and 700003, and the corresponding fluxes (absorbed and unabsorbed) and luminosities (in the 0.2–10 keV band and assuming a distance of 60.6 kpc).

Observation	700001	700003
N_{H} (TBabs, 10^{22})	0.0536 (frozen)	-
N_{H} (TBvarabs, 10^{22})	$0.70^{+0.28}_{-0.23}$	-
Γ	$0.96^{+0.27}_{-0.24}$	-
χ^2	101.9	-
d.o.f	102	-
Flux ^a	$9.40^{+1.68}_{-1.79}$	$8.49^{+0.98}_{-1.39}$
Unabs. Flux ^a	10.09	9.11
Unabs. Lum. ^b	4.43	4.00

^a ($\times 10^{-13}$ erg s $^{-1}$ cm $^{-2}$)

^b ($\times 10^{35}$ erg s $^{-1}$)

tainties). The spectra for all cameras covering the sources (excluding the light-leak cameras TM5 and TM7, Predehl et al. 2021) were fitted using an absorbed power-law and two absorption components (TBabs*TBvarabs*power). TBabs and TBvarabs are the Tuebingen-Boulder ISM absorption model as defined in Wilms et al. (2000). The first absorption component has a fixed Galactic N_{H} value of 5.36×10^{20} cm $^{-2}$ (Dickey & Lockman 1990) and the second N_{H} is left free, while the abundance is fixed to 1.0 for He and 0.2 for Z>2 (Russell & Dopita 1992).

Only the normalization constant for the spectra of different observations was left free. The results of the spectral fit are shown in Fig. 4 together with their residuals, for obsID 700001 (top) and 700003 (bottom). The values of the spectral parameters as well as the observed and unabsorbed fluxes and luminosities (assuming a distance of 60.6 kpc, Hilditch et al. 2005) are shown in Table 1. The observed fluxes are in the range of those reported by Maggi et al. (2013), 0.66 to 2.87×10^{-12} erg cm $^{-2}$ s $^{-1}$, from the *Swift* observations mentioned in Sec. 1, where count rates were converted into 0.3–10 keV fluxes assuming an absorbed power-law model with $N_{\text{H}}=1 \times 10^{21}$ cm $^{-2}$ and $\Gamma=1$. Besides the Galactic foreground absorbing column density, which at those coordinates is $N_{\text{H}}=5.36 \times 10^{20}$ (using the N_{H} online calculator³), there is some additional X-ray absorption arising in the interstellar medium of the SMC or close to the source. The power-law index derived here is consistent with what is retrieved for other SMC Be/X-ray binaries. An average value of 0.93 was reported in Haberl et al. (2008) (90% of the values being between 0.71 and 1.27), based on *XMM-Newton* observations of 20 Be/X-ray binaries with luminosities above 10^{35} erg s $^{-1}$, for which spectral fitting was possible.

Taking into account the large uncertainties, fluxes are consistent between the two observations, indicating that the source is not varying significantly on a time scale of a few days.

3.2. SALT-RSS spectrum

Fig. 5 shows the optical spectrum of XMMU J010429.4–723136 taken with SALT-RSS. The spectrum is dominated by a single-peaked, slightly asymmetric H α emission line, with a steeper

² <https://heasarc.gsfc.nasa.gov/xanadu/xspec/python/html/index.html>

³ <https://heasarc.gsfc.nasa.gov/cgi-bin/Tools/w3nh/w3nh.pl>

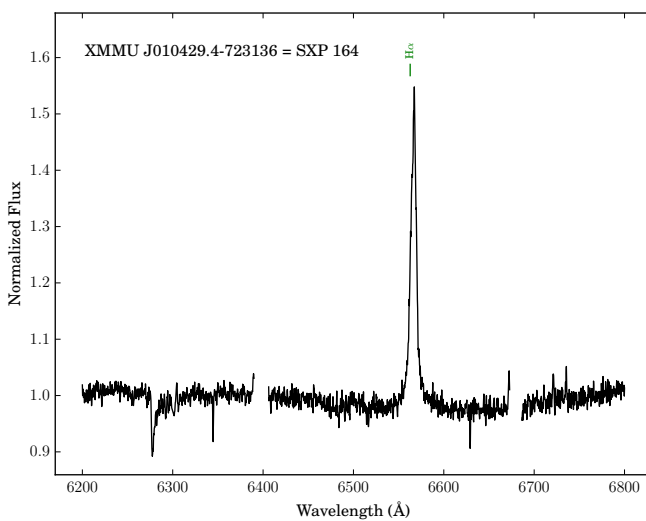


Fig. 5. Optical spectrum of XMMU J010429.4–723136 obtained on 2019-11-24, using the Robert Stobie Spectrograph on SALT. The rest wavelength of the H α line is marked.

gradient on the red-ward side. The measured line properties are: E.W. = -5.12 ± 0.14 Å, FWHM = 7.224 ± 0.023 Å and central position of the H α line = 6566.358 ± 0.028 Å (corrected to the solar system barycenter).

3.3. OGLE data and orbital period search

The upper part of Fig. 6 shows the OGLE light curve, in the I band, as provided in the xrom data archive. The observations cover the period ranging from May 2010 to January 2020. The source is first at low flux level for the first ~ 600 d and then increases into a high state, on a time scale of ~ 1 yr (from November 2011 to October 2012), where it stays until the end of the observations. In an attempt to look for a periodic signal, possibly associated with the orbital period, we detrended the light curve using a hamming window function (with Python tool PyAstronomy.pyasl.smooth) and removed the data points where the flux abruptly increases. The resulting light curve is shown in the middle of Fig. 6. Finally, the bottom part shows the portion of the light curve with the source in the bright state only, representing a large fraction of the data (with respect to its fainter state).

On each light curve a period search was performed using the same Lomb-Scargle analysis as in Sec 3.1.1, in the period range from 10 to 50 d, and results are shown in Fig. 7. For the full light curve, the maximum peak is found at 22.09 ± 0.04 d but not very pronounced (confidence levels using the bootstrap method can't be used because of the flux increase). For the detrended or high flux only light curves the best period is found at 22.35 ± 0.11 d in both cases and the signal is significant at least at 90% confidence level. Note that for the detrended light curve, a change of the window width of the smooth algorithm would slightly change the shape of the periodogram, but the best period value would still be consistent within the error bars and the significance of the peak would still be above 99%. Furthermore, no other significant peak is found between 50 d and 150, for the detrended and high flux only light curves.

The detrended light curve folded at the best period is shown in Fig. 8, where Phase 0 corresponds to the start of the observation (MJD: 55378.44102). The shape is symmetric and has more

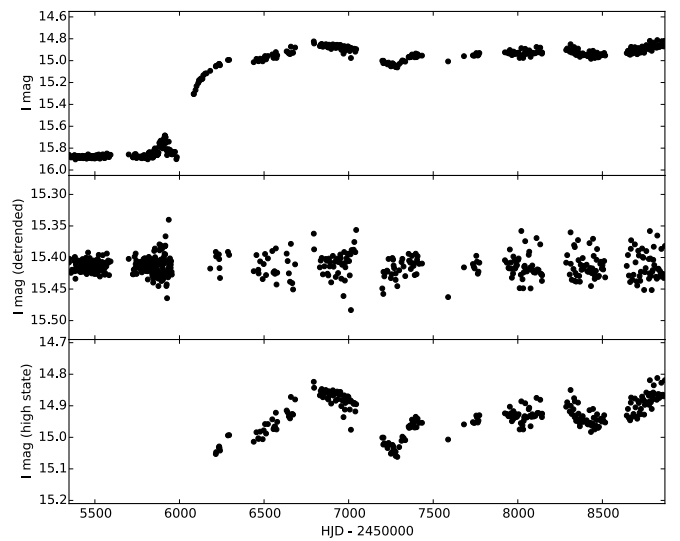


Fig. 6. OGLE light curve of SXP 164, in the I band: full light curve (top), detrended (middle), high state only (bottom).

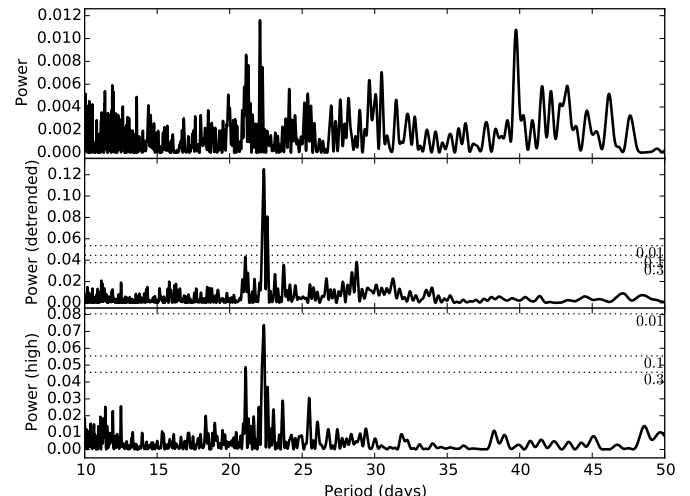


Fig. 7. Lomb-Scargle periodogram of the OGLE full (top), detrended (middle), high state only (bottom) light curve showing a clear peak at 22.35 d for the detrended and high-state light curve (22.09 d in the full light curve). The confidence levels (given at 68%, 90% and 99%) are derived using the block-bootstrap method.

a sinusoidal than a FRED-like (Fast Rise Exponential Decay) profile (see Bird et al. 2012, for a comparison between both profiles). FRED-like profiles for orbital modulations are expected in Be-X-ray binaries, which would be caused by the neutron star disturbing the circumstellar disc of the Be star.

3.4. Long-term X-ray light curve

Figure 9 shows the long-term X-ray light curve of SXP164, in the time interval covered by the OGLE monitoring (shown again at the bottom). The measured 0.2–12 keV fluxes (dots) and the upper limits (red triangles) are derived from both pointed and slew *XMM-Newton* and *Swift* observations using the Upper Limit Server (ULS⁴). The values are derived assuming a power-law spectrum with $N_{\mathrm{H}} = 1 \times 10^{21} \mathrm{cm}^{-2}$ and a spectral index $\Gamma=1$,

⁴ <http://xmmluls.esac.esa.int/upperlimitserver>

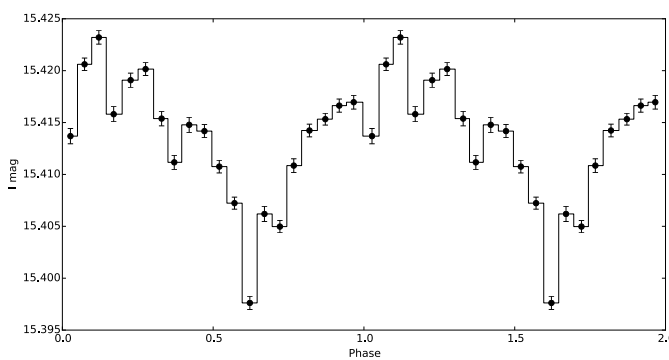


Fig. 8. Detrended OGLE light curve folded at the best period, the shape being symmetric and having more a sinusoidal than a FRED-like profile.

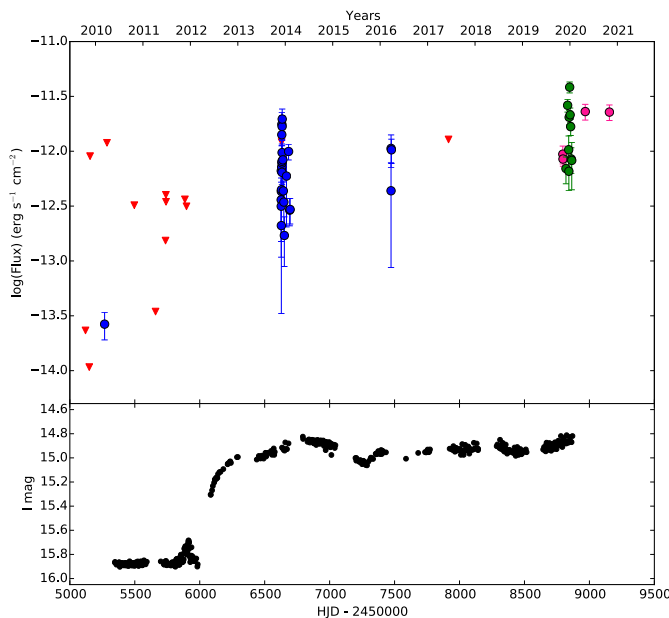


Fig. 9. Long-term X-ray light curve of SXP164 during the OGLE monitoring (bottom). Dots represent measured flux, while upper limits are shown as red triangles. Values from early observations are derived using the Upper Limit Server, ULS (*XMM-Newton* and *Swift* data), while eROSITA fluxes and latest *Swift* measurements (not included in the ULS) are shown in pink and green, respectively.

as in Maggi et al. (2013). Chandra observed the source only once, in August 2002, where the flux was 3.2×10^{-13} erg cm $^{-2}$ s $^{-1}$ (Rajoelimanana et al. 2011a). The 0.2-10 keV fluxes from the most recent *Swift* observations (1 December 2019 to 15 Januray 2020), which are not included in the ULS, are shown in green and assume the same spectral model. Besides the pointed observations described in this paper, the source was observed as well during the eROSITA all-sky surveys eRASS1 (in April/May 2020) and eRASS2 (in November 2020) with a average count rate of 0.269 ± 0.044 cts s $^{-1}$ and 0.226 ± 0.043 cts s $^{-1}$ (successive ~ 40 s observations separated by ~ 4 hrs gaps). The count rates are converted in fluxes using the same scaling factor as for the pointed observations. The resulting eROSITA fluxes, as derived in Sec.3.1.2 and from the surveys are shown in pink.

The long-term light curve indicates the possibility that the source became bright simultaneously in the X-ray and the I bands, i.e. from late 2012. Some variability (a factor of ~ 10) is nevertheless present in the high X-ray state.

4. Discussion

We report here the discovery of the pulse period (164 s) and possibly the orbital period (22 d) of a known Be/X-ray binary in the SMC. As for many other ones belonging to that galaxy, the source is highly variable in the X-rays with a ratio $F_{\text{max}}/F_{\text{min}} \gtrsim 750$ with $F_{\text{max}} \sim 3.8 \times 10^{-12}$ and $F_{\text{min}} \lesssim 5 \times 10^{-15}$ erg cm $^{-2}$ s $^{-1}$ (upper limit from a *XMM-Newton* observation performed in October 2000). Those values are in line with what is reported in Haberl & Sturm (2016), in their Fig. 5 for the other SMC Be/X-ray binaries.

According to the well-known Corbet diagram (Corbet 1986), an empirical power-law relationship between the pulse period P_s (in seconds) and the orbital period P_o (in days) was derived for Be/X-ray binaries, based on the observed values, with e being the orbital eccentricity:

$$P_o = 10(1 - e)^{-3/2} P_s^{0.5} \quad (1)$$

A more recent, and updated version of this empirical relationship was proposed by Yang et al. (2017) as:

$$P_o = 12.066 P_s^{0.425} \quad (2)$$

This relationship can be explained for systems being in a state of quasi-equilibrium in which the Alfvén radius (the radius where the inflowing matter couples to the magnetic field lines of the neutron star) and corotation radius (radius where the spin angular velocity of the neutron star is equal to the Keplerian angular velocity) are, on average, equal. In the Corbet diagrams however a large scatter is observed in both papers, as it is also shown in Haberl & Sturm (2016), indicating that probably many systems are not in a state of quasi-equilibrium, hence having their pulse period still varying. Assuming a circular orbit, a pulse period of 164 s would lead to an orbital period of 128 d (equ. 1) or 105 d (equ. 2), which is much longer than what is derived here from the OGLE data. On the other hand, an orbital period of 22.3 d would lead to an equilibrium pulse period of 5.0 s (equ.1) or 4.2 s (equ.2), suggesting that the neutron star can still considerably spin-up in the future. SXP1323 had, for example, a stable pulse period around 1323 s from 2000 to 2006, and then started to spin-up rapidly from 2006 to 2016 while keeping a constant flux (Carpano et al. 2017), to reach 1005 s in November 2019 (Haberl et al. 2019).

The comparison of the system's long-term X-ray and OGLE light curves indicates that the flux growth in both wavelength bands are correlated. The long-term optical variations of Be/X-ray binaries are believed to be related to the formation and depletion of the circumstellar disc around the donor star, giving rise to the Be phenomenon, as suggested in Rajoelimanana et al. (2011b). A larger disc, could lead to a higher accretion rate onto the neutron star and therefore increase its X-ray luminosity. Since eROSITA is the only instrument that has observed the source in its bright state, with a sufficiently long exposure to retrieve the pulse period, it is currently not possible to know the long-term impact of a larger Be disc on the pulse period derivative and new pointed observations are therefore required.

The optical spectrum is dominated by the H α emission line, emitted from the circumstellar disc surrounding the Be star, and is therefore a good probe of the disc. The presence of the H α emission line is one of the main classification criteria for Be/X-ray binaries. In Coe & Kirk (2015); Antoniou et al. (2009), it is shown that a strong correlation exists between the orbital period P_{orb} (d) and the line equivalent width (\AA). The linear best fit de-

rived from the EW/P_{orb} distribution of Be/X-ray pulsars in the SMC, gives the relationship:

$$H_{\alpha}\text{EW}(\text{\AA}) = [-0.16 \times P_{\text{orb}}] - 9.7 \quad (3)$$

for orbital periods $P_{\text{orb}} \leq 150$ d (Coe & Kirk 2015, see their Fig. 8). This would lead to an $H_{\alpha}\text{EW} = -13.3$ Å for a period of 22.35 d, which is somewhat larger than what is retrieved from the SALT spectral fit (-5.12 ± 0.14 Å). This difference could be explained on one hand, by the large scatter in the EW/P_{orb} distribution, especially for the short period systems, and on the other hand because the relationship makes use of the maximum EW ever measured (indicating how large a disc can possibly grow). It may be that the SALT EW measurement reported here was performed when the disc hadn't reached its maximum size and the OGLE period of 22.3 d is therefore still possibly associated to the orbital period. The EW/P_{orb} relationship is explained by the disc of the Be star being truncated by the neutron star during its orbit. The neutron star appears to act as a barrier, preventing the formation of an extended disc in systems with short orbital periods. This should also imply that the circumstellar disc, and in turn the H_{α} EW, are on average smaller in binary systems than for isolated Be stars. Correlations between the spectral parameters of the H_{α} line and rotational velocity have been observed in many Be stars and are interpreted as evidence for rotationally dominated circumstellar discs (Dachs et al. 1986; Hanuschik et al. 1988; Reig 2011). A monitoring of the H_{α} EW and profile, over a period of few months, could on one hand confirm the 22.3 d orbital period as well as providing constraints on the inclination angle of the Be disc.

Acknowledgements. This work is based on data from eROSITA, the primary instrument aboard SRG, a joint Russian-German science mission supported by the Russian Space Agency (Roscosmos), in the interests of the Russian Academy of Sciences represented by its Space Research Institute (IKI), and the Deutsches Zentrum für Luft- und Raumfahrt (DLR). The SRG spacecraft was built by Lavochkin Association (NPOL) and its subcontractors, and is operated by NPOL with support from the Max Planck Institute for Extraterrestrial Physics (MPE). The development and construction of the eROSITA X-ray instrument was led by MPE, with contributions from the Dr. Karl Remeis Observatory Bamberg & ECAP (FAU Erlangen-Nürnberg), the University of Hamburg Observatory, the Leibniz Institute for Astrophysics Potsdam (AIP), and the Institute for Astronomy and Astrophysics of the University of Tübingen, with the support of DLR and the Max Planck Society. The Argelander Institute for Astronomy of the University of Bonn and the Ludwig Maximilians Universität Munich also participated in the science preparation for eROSITA. The eROSITA data shown here were processed using the eSASS/NRTA software system developed by the German eROSITA consortium. The optical spectrum presented in this paper were obtained with the Southern African Large Telescope (SALT).

Dickey, J. M. & Lockman, F. J. 1990, *ARA&A*, 28, 215
 Galache, J. L., Corbet, R. H. D., Coe, M. J., et al. 2008, *ApJS*, 177, 189
 Haberl, F., Carpano, S., Maitra, C., et al. 2019, *The Astronomer's Telegram*, 13312, 1
 Haberl, F., Eger, P., & Pietsch, W. 2008, *A&A*, 489, 327
 Haberl, F. & Sturm, R. 2016, *A&A*, 586, A81
 Hanuschik, R. W., Kozok, J. R., & Kaiser, D. 1988, *A&A*, 189, 147
 Hilditch, R. W., Howarth, I. D., & Harries, T. J. 2005, *MNRAS*, 357, 304
 Lomb, N. R. 1976, *Ap&SS*, 39, 447
 Maggi, P., Sturm, R., Haberl, F., & Vasilopoulos, G. 2013, *The Astronomer's Telegram*, 5674, 1
 McBride, V. A., González-Galán, A., Bird, A. J., et al. 2017, *MNRAS*, 467, 1526
 Predehl, P., Andritschke, R., Arefiev, V., et al. 2021, *A&A*, 647, A1
 Rajoelimanana, A. F., Charles, P. A., & Udalski, A. 2011a, *The Astronomer's Telegram*, 3154, 1
 Rajoelimanana, A. F., Charles, P. A., & Udalski, A. 2011b, *MNRAS*, 413, 1600
 Reig, P. 2011, *Ap&SS*, 332, 1
 Russell, S. C. & Dopita, M. A. 1992, *ApJ*, 384, 508
 Scargle, J. D. 1982, *ApJ*, 263, 835
 Schmidtke, P. C., Cowley, A. P., & Udalski, A. 2013, *MNRAS*, 431, 252
 Sturm, R., Haberl, F., Pietsch, W., et al. 2013, *A&A*, 558, A3
 Udalski, A. 2008, *Acta Astron.*, 58, 187
 Wilms, J., Allen, A., & McCray, R. 2000, *ApJ*, 542, 914
 Yang, J., Laycock, S. G. T., Christodoulou, D. M., et al. 2017, *ApJ*, 839, 119

References

Antoniou, V., Hatzidimitriou, D., Zezas, A., & Reig, P. 2009, *ApJ*, 707, 1080
 Bird, A. J., Coe, M. J., McBride, V. A., & Udalski, A. 2012, *MNRAS*, 423, 3663
 Brunner, H. et al., submitted
 Buckley, D. A. H., Swart, G. P., & Meiring, J. G. 2006, in *Society of Photo-Optical Instrumentation Engineers (SPIE) Conference Series*, Vol. 6267, Society of Photo-Optical Instrumentation Engineers (SPIE) Conference Series, ed. L. M. Stepp, 62670Z
 Burgh, E. B., Nordsieck, K. H., Kobulnicky, H. A., et al. 2003, in *Society of Photo-Optical Instrumentation Engineers (SPIE) Conference Series*, Vol. 4841, *Instrument Design and Performance for Optical/Infrared Ground-based Telescopes*, ed. M. Iye & A. F. M. Moorwood, 1463–1471
 Carpano, S., Haberl, F., & Sturm, R. 2017, *A&A*, 602, A81
 Coe, M. J., Edge, W. R. T., Galache, J. L., & McBride, V. A. 2005, *MNRAS*, 356, 502
 Coe, M. J. & Kirk, J. 2015, *MNRAS*, 452, 969
 Corbet, R. H. D. 1986, *MNRAS*, 220, 1047
 Dachs, J., Hanuschik, R., Kaiser, D., et al. 1986, *A&AS*, 63, 87